

# Control and generation of localized pulses in passively mode-locked semiconductor lasers

M. Marconi, J. Javaloyes, P. Camelin, D. Chaparro, S. Balle, and M. Giudici *Member, IEEE*.

**Abstract**—We show experimentally and theoretically that localized pulses can be generated from an electrically biased 200  $\mu\text{m}$  multi-transverse mode Vertical-Cavity Surface-Emitting Laser. The device is passively mode-locked using optical feedback from a distant Resonant Saturable Absorber Mirror and it is operated below threshold. We observe multistability between the off solution and a large variety of pulsating solutions with different number and arrangements of pulses per round-trip, thus indicating that the mode-locked pulses are localized, i.e. mutually independent. We show that a modulation of the bias current allows controlling the number of the pulses travelling within the cavity, thus suggesting that our system can be operated as an arbitrary pattern generator of 10 ps pulses and 1 W peak power.

**Index Terms**—Mode-Locking, Broad-Area Lasers, VCSELs

## I. INTRODUCTION

Mode-locking (ML) is a fascinating phenomenon that allows the generation of ultrashort pulses from a laser [1] and that is still a subject of intense research. Passive ML (PML) is arguably the most successful approach and it is achieved by combining two elements, a laser amplifier which provides gain and a saturable absorber (SA) acting as a pulse shortening element, see [1] for a review. Pulsed emission with a fundamental period corresponding to the cavity round-trip time arises from the different dynamical properties of the SA and the amplifier, which open a short window for amplification around the pulse [2], [3]. ML has led to the shortest and most intense optical pulses ever generated and pulses in the femtosecond range are produced by dye [4] and solid state lasers [5]. Large output powers in the Watt range are commonly achieved from coupled VCSELs-SESAM [6] configurations. On the other hand, the large gain of semiconductor materials allows building sub-millimeter Monolithic PML lasers. The round-trip of such short devices is typically of the order of 10 ps and they can therefore reach repetition frequencies of several tens of GHz. They have also the advantage of being compact, low cost and adaptable to many cavity geometries [7], yet their power is in the milli-Watt range.

In spite of the research efforts dedicated to the general understanding of the basic issues, several aspects of PML still

represent a scientific challenge. For instance, while the breadth of the active medium gain curve is well known to govern the pulse-width, it was only very recently understood that the SA also provides a strongly asymmetric and non linear filtering. Such an usually overlooked effect was recently proven to be the key mechanism explaining wavelength instabilities in PML lasers [8], [9]. In addition, recent studies indicated that the optimal position of the SA in the cavity was not following intuitive rules [10]. Similarly, it was commonly thought until recently that PML semiconductor lasers can not operate at low repetition rates due to the fast recovery time of their material gain ( $\tau_g \sim 1$  ns) which should limit them to high repetition frequencies ( $\gtrsim 1$  GHz). Too long cavities result in the so-called regime of harmonic mode-locking in which several pulses circulate in the cavity, according to the background stability criterion [1]. Until recently, the record of the lowest frequency PML was experimentally attained around  $\sim 300$  MHz [11], [12], [13].

We have recently shown that, in the limit of cavity round-trip much longer than the gain recovering time, mode-locked pulses may coexist with the zero intensity background and can be interpreted as *temporal Localized Structures* (LS) [14]. Localized pulses can be independently addressed and used as elementary bits of information, hence the cavity can be used as an all-optical buffer, as shown in [15]. A single localized pulse can be activated within the cavity, independently from the cavity size, thus leading to arbitrary low repetition rates which allowed establishing a new low frequency record of 65.5 MHz [14]. The possibility of addressing individually localized pulses opens interesting possibilities for the optical generation of arbitrary trains of narrow pulses, which has a large number of potential applications in different domains, e.g. time-resolved spectroscopy, pump-probe sensing of material properties, generation of frequency combs, Optical Code Division Multiple Access Communication Networks [16] and LIDAR [17], [18].

In this manuscript, we show how localized pulses form in a passively mode-locked semiconductor broad-area VCSEL coupled to a resonant saturable absorber mirror (RSAM). The VCSEL bias current is used as a control parameter for addressing localized pulses and for generating patterns of closely packed narrow pulses. The experimental evidences and theoretical analysis pave the path towards an optical arbitrary pattern generator of short light pulses.

M. Marconi, P. Camelin and M. Giudici are with the Institut Non Linéaire de Nice, Université de Nice Sophia Antipolis - Centre National de la Recherche Scientifique, 1361 route des Lucioles, F-06560 Valbonne, France, e-mails: [mathias.marconi@inln.cnrs.fr](mailto:mathias.marconi@inln.cnrs.fr), [patrice.camelin@inln.cnrs.fr](mailto:patrice.camelin@inln.cnrs.fr) and [masimo.giudici@inln.cnrs.fr](mailto:masimo.giudici@inln.cnrs.fr).

D. Chaparro and J. Javaloyes are with the Departament de Física, Universitat de les Illes Balears, C/ Valldemossa, km 7.5, E-07122 Palma de Mallorca, Spain, e-mail: [daniel.chaparro@uib.es](mailto:daniel.chaparro@uib.es) and [julien.javaloyes@uib.es](mailto:julien.javaloyes@uib.es)

S. Balle is with the Institut Mediterrani d'Estudis Avançats, CSIC-UIB, E-07071 Palma de Mallorca, Spain, e-mail: [salvador@imedea.uib-csic.es](mailto:salvador@imedea.uib-csic.es)

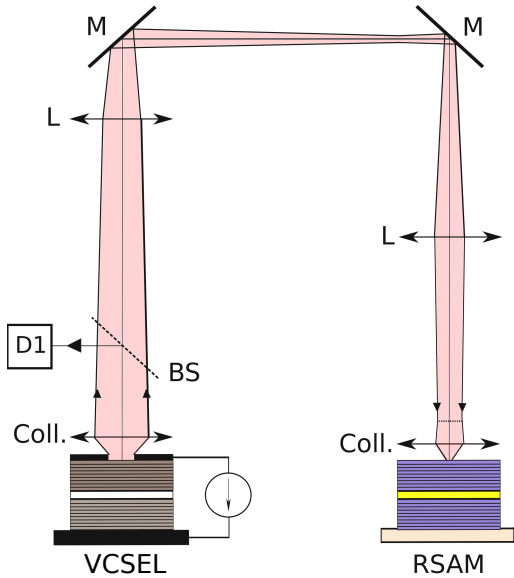


Figure 1. Experimental Set-up: Temperature-stabilized VCSEL and RSAM. Coll.: Aspheric Lens, BS : Beam Splitter, M: Mirror and D1: Detector and CCD cameras.

## II. EXPERIMENTAL RESULTS

### A. Experimental setup

Our VCSEL is a 980 nm device manufactured by ULM Photonics [19]. Its standalone threshold current ( $J_{st}$ ) is about 380 mA, though emission is localized only at the periphery of the device up to  $J = 850$  mA, after which roll-off starts to occur. The 980 nm RSAM (BaTop GmbH) has a transverse dimension of  $4 \times 4$  mm<sup>2</sup> and it exhibits a low unsaturated reflectivity of 1% that increases up to 60% when saturated. The RSAM saturation fluence is  $15 \mu\text{J}\cdot\text{cm}^{-2}$ . These values are obtained at the RSAM resonant wavelength which can be thermally tuned over 3 nm (between  $T_1 = 10$  °C and  $T_2 = 50$  °C). The Full Width at Half Maximum (FWHM) of the RSAM resonance is around 16 nm and the saturable absorption recovery time is around 1 ps. The setup is shown in Fig. 1. Both the VCSEL and RSAM are mounted on temperature controlled substrates which allow for tuning the resonance frequency of each cavity; parameters are set for having the emission of the VCSEL resonant with the RSAM. The light emitted by the VCSEL is collected by a large numerical aperture (0.68) aspheric lens and a similar lens is placed in front of the RSAM. A 10% reflection beam splitter allows for light extraction from the external cavity and to monitor both the VCSEL and the RSAM outputs. Intensity output is monitored by a 33 GHz oscilloscope coupled with fast 10 GHz detector. Part of the light is sent to two CCD cameras; the first one records the near-field profile of the VCSEL, while the second records the VCSEL's far-field profile. The external cavity length round-trip ( $\tau$ ) is fixed at  $\tau = 15$  ns which corresponds to a 66.6 MHz fundamental repetition rate.

### B. From conventional mode-locking to localized pulses

The combination of the VCSEL and the RSAM in self-imaging condition does not induce an appropriate ratio of

the saturation parameters for obtaining PML. Notwithstanding, mode-locking was obtained when placing the RSAM surface in the exact Fourier transform plane of the VCSEL near-field profile, i.e. when imaging the VCSEL far-field profile onto the RSAM surface [20]. As a consequence, the VCSEL profile was imaged onto itself after a single external cavity round-trip, but inverted (i.e. a magnification factor of  $-1$ ). As shown in [20], such configuration leads to the generation of two opposed tilted plane waves, i.e. waves that have a propagation wave-vector slightly out of the cavity axis  $z$  and which travel in the external cavity with an opposite transverse component and alternating each other at every round-trip. Each one of these plane waves gives birth to a train of mode-locked pulses separated by twice the external cavity round-trip ( $2\tau$ ), while the two trains are time shifted of  $\tau$ . Intuitively, one understands that injecting the Fourier transform of the VCSEL near-field profile into the RSAM strongly favors the emission of a tilted wave from all points of the VCSEL, since the Fourier transform of such an emission consists in a tight focused single spot that saturates easily the RSAM. While this scheme leads to conventional mode-locking and harmonic mode-locking for cavity lengths and round-trips shorter than the gain recovery time ( $\tau < \tau_g$ ), we operate the system in the regime of long cavities, i.e.  $\tau \gg \tau_g$ , and for bias currents below the laser threshold. In these conditions, as shown in [14], several emission states, including the zero intensity (off) solution, coexist for the same values of bias current.

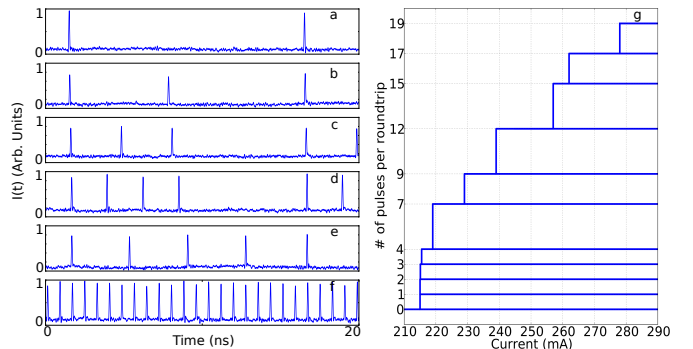


Figure 2. Left: Examples of coexisting time output traces for  $J = 280$  mA and  $\tau = 15$  ns. The panels a), b), c) and d) correspond to  $N = 1, 2, 3, 4$  pulses per round-trip, respectively. Another configuration for  $N = 4$  is shown in e) where the pulses are regularly distributed within the cavity. The maximal number of pulse is  $N = 19$  as depicted in panel f). Right: experimentally obtained bifurcation diagram for the number of pulses per round-trip (g) as a function of the bias current. The stability of each solution is indicated by the solid horizontal lines.

These emission states are characterized by a different number of pulses circulating in the cavity, and for the same number of pulses, a large variety of pulse arrangement can be observed. In Fig. 2a-d) few examples between the large number of coexisting emission states is represented, including  $N = 1, 2, 3$  and 4 pulses circulating inside the cavity. For the  $N = 4$  pulses case, we show two situations where they appear either grouped, see Fig. 2d), or equally separated Fig. 2e). The case of  $N = 19$  pulses circulating within the cavity represents the largest number of pulses that can be obtained for the size of the external cavity chosen. All the above listed pulsing

solutions coexist in the parameter space for a wide range of VCSEL pumping current  $J$ . The pulse width cannot be determined precisely from the oscilloscope traces shown in Fig. 2, which are limited by our real-time detection system (10 GHz effective bandwidth). However, an estimation of the pulse width can be obtained from the optical spectrum of the output, which exhibits a broad spectral peak whose FWHM is around 0.12 nm that corresponds, assuming a time-bandwidth product of 0.4, to a pulse width of 10 ps FWHM. The pulse was also detected by a 36 GHz detector, which confirms a pulse width of less than 12 ps FWHM considering the oscilloscope bandwidth limit. Finally, the pulse peak power has been measured to be 1 Watt.

The multistability between a large number of different solutions is shown in Fig. 2g), where we plot the bifurcation diagram of these solutions as a function of the pumping current. Figure 2g) is obtained increasing the parameter  $J$  from  $J = 210$  mA, where only the steady off solution is stable, up to the value where this solution loses its stability ( $J < 350$  mA) and then sweeping it down until a periodic emission with  $N = 19$  pulses per round-trip appears, see Fig. 2f). In analogy to spatial localized structures [21], [22], this state corresponds to the fully developed temporal pattern which is, together with the coexisting stable off solution, at the origin of the localized structures. As  $J$  is decreased, the state with  $N = 19$  pulses per round-trip loses its stability and the system bifurcates progressively towards states with smaller numbers of LS, until a single one is present in the cavity. Each state is spontaneously appearing as  $J$  is scanned downward and, once a new state appears, we increase  $J$  to explore its stability up to  $J = 290$  mA. As far as the system remains on the same branch there is no change in the pulse arrangement, thus showing that, even if several arrangements are possible, once one is chosen, it is stable versus parameter changes. Figure 2 indicates that in this regime, mode-locked pulses in our system can be interpreted as temporal localized structures, i.e. any pulse is independent from the other and it can be individually addressed. It is worthwhile noting that the localized character of the pulse implies that the pulse is localized not only in the intensity but also in all the variables describing the system. This means that, after the short intensity pulse emission, the gain and saturable loss variables recover their steady state value on a longer time scale thereby defining the effective temporal extent of the LS. This is the main difference between localized pulses and conventional mode-locked pulses. In the latter case, which is obtained for pumping levels above laser threshold, the gain does not recover to its steady state value between pulses. This is well explained by the background stability criterion [1] which states that a pulsating solution is stable if losses are larger the gain between pulses. Since the laser is pumped above threshold, the only stable pulsating solution is the one having a number of pulses in the cavity large enough such that, in-between pulses, gain cannot recover sufficiently to overcome the unsaturated loss level. This implies that fundamental mode-locking is possible only for  $\tau < \tau_g$ . In the case of localized pulses, we are in the opposite limit and the gain can recover fully between pulses because the maximal gain level remains below the unsaturated

loss level, even for an infinitely long interval between pulses. Thus, localized PML pulses have no lower limit in their repetition rate, as shown in Fig. 2a) where a repetition rate of 66.6 MHz is obtained. On the other hand, the recovery time of the slowest variable, in our case the gain recovery time, determines the effective temporal extent of the localized pulse, since no other pulse can occur before the recovery of all the variables. Another important difference between localized pulses and conventional mode-locked pulses is that, for a given set of parameters, the energy of the localized pulses does not depend significantly on the number of pulses circulating inside the cavity. Instead in conventional mode-locking the energy of the system is shared between the pulses which circulate inside the cavity and fundamental mode-locking is preferred over harmonic mode-locking for maximum pulse energy.

In order to represent the evolution of the localized pulses travelling within the cavity over many round-trips, we use the so-called space-time diagram representation where the temporal trace is folded onto itself at the cavity round-trip period. Accordingly, the round-trip number  $n$  becomes a pseudo-time variable while the pseudo-space variable corresponds to the timing of the pulse modulo  $\tau$ . This representation is similar to the one used for following the evolution of pulses along optical fibers where fast and slow time scales are well separated and it has been proposed also for delayed system [23], [24], [25]. In Fig. 3a-d) we show some space-time like diagrams obtained from the same time traces used for Fig. 2 where all the situations depicted coexist for the same parameter values. Panel a) shows the evolution of a single LS in the external cavity, while panel b), c) and d) represent the evolution of respectively  $N = 3, 4$  and 19 pulses. In all the situations, the pulses do not visibly jitter over the considered timescale of  $6.5 \times 10^3 \tau \sim 100 \mu\text{s}$  and they seems to be insensitive to the surrounding noise. This can be attributed to the presence of the saturable absorber which acts as an effective noise eater. While the RSAM opens a very short window of net gain around the pulse, the remaining low intensity emission from the VCSEL is absorbed by the RSAM. Accordingly, the background shown in Fig.3 is homogeneous and corresponds to zero emission.

In presence of localized structures, as the ones shown in Fig. 3, the possibility of forming bounded states of localized structures, also called molecules, naturally arises. When gath-

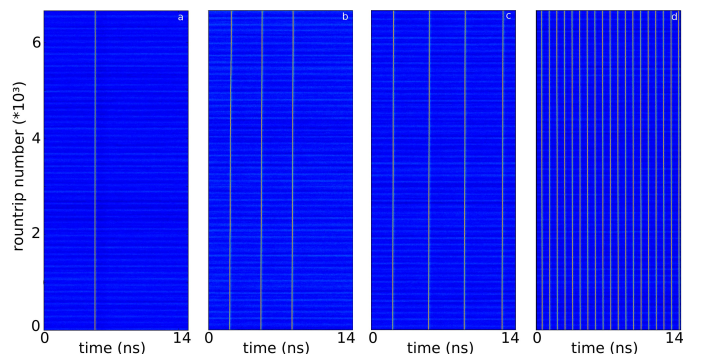


Figure 3. Space-time like diagrams obtained. a) a single pulse per round-trip, b) three pulses, c) four regularly spaced pulses and d) nineteen pulses as in Fig. 2 f).

ered in molecules, the pulses are not independent anymore, while the molecule itself becomes a compound localized structure which is independent from other localized structures that may travelling within the cavity. Such molecules have been widely observed in fiber lasers [26] and in general only a few if not an unique equilibrium distance separates the “atoms” of a molecule. The signature of such bound states of LS in a space-time like diagram is the presence of preferred distances between two neighbor pulses. We have never found any preferred distances between close pulses in the space-time like diagrams that we have analyzed. Instead we have observed a *continuum* of temporal separations. One can understand the absence of molecules in our system by the specificity of the interaction between neighbor LS. Indeed, it is known that the gain depletion induced by each LS produces a repulsive interaction [27] that decays over a time scale  $\tau_g$ . The potentially attractive interaction mediated by the oscillating tails of the pulses vanishes after a few times the effective pulse width, i.e. a time scale of  $\sim 30$  ps. As such, this clear scale separation between the attractive and repulsive forces explain why LS molecules would be hard to obtain with semiconductor active materials.

It may be useful to compare our results with the extensive literature on mode-locking. Localized pulses in mode locked laser might have been observed in the past. For example, several papers mention PML regimes obtained at *exceedingly low* frequencies with respect to the limits of the background stability criterion; repetition rates of the order of few hundreds MHz were reported in [11], [12], [13]. We believe that these regimes could be explained in terms of LS. While it is difficult to know exactly the experimental conditions of these works, in [11] it is clearly mentioned that the off solution coexists with the PML solution. The experimental result reported recently in [28], claiming mode-locking at a repetition rate of 85.7 MHz, can also be explained in terms of LS. In this work, neighboring pulses of 50 ps FWHM, separated of 1 ns, are interpreted theoretically as bound states. While the experimentally observed distance corresponds to the vanishing of the repulsive interaction induced by the gain depletion [27], the theoretical analysis is performed after adiabatically eliminating the carrier dynamics, thus neglecting such repulsive interactions. We believe that this approximation in [28], correct for fiber lasers but not for semiconductor devices, has led to a wrong interpretation of independent neighbor pulses in terms of bound states resulting of the locking of the oscillating tails of the pulses.

### C. Localized pulse addressing

The most important property of localized structures is their mutual independence which allows for their individual addressing. The localized pulses that we have obtained can be individually triggered by shining light pulses inside the cavity, as we have shown numerically in [14]. By encoding an information bit in the form of a localized pulse, our system can be operated as an all-optical buffer, similar to the one proposed using fiber Kerr resonator with a driving field [15], but taking advantage of the compactness and fast response of

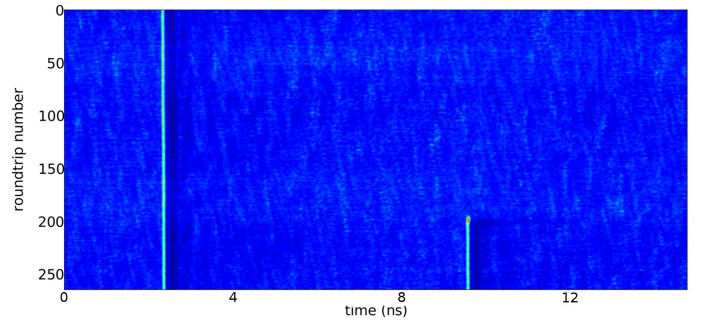


Figure 4. Space-time like diagram showing nucleation of a localized pulse after a mechanical perturbation of the system. Parameters are in the multi-stable region of Fig. 2

semiconductor materials as in [25]. The buffer bit-rate depends on the minimal time interval between two independent pulses, i.e. the temporal extent of the LS which is, in our case, fixed by the gain recovery time. The experimental results shown in Fig. 2f) indicate that a separation of 1 ns is certainly sufficient to avoid interaction between pulses, thus leading to buffer bit rate of  $\sim 1$  GHz. While the all-optical addressing of the mode-lock localized pulses is the topic of ongoing research, the nucleation of a single pulse can be observed when perturbing mechanically the system, as shown in Fig. 4. Yet this kind of perturbation does not allow any control of the switching; it may lead to the nucleation of several pulses at the same time with random positions within the cavity.

Notwithstanding, a higher degree of control can be implemented when perturbing the bias current of the VCSEL. The main limitation using this parameter comes from the frequency response of the VCSEL to a modulated signal coupled onto the pumping current via a bias T. The electrical characteristics of the broad-area VCSEL we used, together with the bandwidth of the bias-T used, limit the frequency modulation below 0.3 GHz. Accordingly, the individual addressing of localized pulses via the emission of electrical pulses suffers from the too long rise time of the perturbation. Nevertheless a sinusoidal modulation of the pumping current with a period corresponding to the cavity round-trip  $\tau$  allows for the excitation of localized pulses in a narrow time interval within the round-trip time, i.e. a well-defined vertical band of the space-like variable, as plotted in Fig. 3. The idea would be to modulate the current between a lowest value where the off solution is the only possible solution up to a highest value where the fully developed temporal pattern shown in Fig. 2f) is also the unique possible situation. Since this modulation is synchronous with the cavity round-trip, a portion of this monostable temporal pattern will appear only in correspondence with the modulation signal peak. Once the sinusoidal perturbation of the pumping current is removed, the portion of the monostable pattern will give way to a solution with one, two or more localized pulse depending on the continuous bias current value of the VCSEL, see Fig. 2g), and on the size of the the temporal pattern excited. The result of this experiment is shown in Fig. 5 where the VCSEL is biased at  $J = 215$  mA, a current value for which for the sake of simplicity only the state with a single localized

pulse per round-trip coexists with the off state. We prepare the system in the off state and then we apply a modulation having a peak to peak amplitude of 460 mA. In correspondence with the modulation peak (where  $J = 445$  mA), six localized pulses appear at a distance of 800 ps, which corresponds to the interpulse distance of Fig. 2f), i.e.  $\sim \tau/19$ . Once the modulation signal is removed, the continuous value of pumping current does not support the stable existence of six localized pulses and the system bifurcates towards the state with a single pulse per period. This regime is stable and it persists indefinitely.

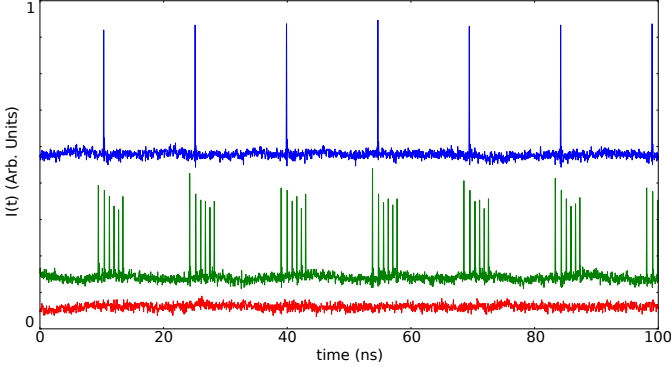


Figure 5. Time traces showing the experimental process for LS generation via current modulation. First the laser is in the 0-LS state without modulation (red, bottom line) and  $J = 215$  mA. Second, modulation is applied with a peak-to-peak amplitude of 460 mA and 6 LS appear close to the peak of the modulation (green, middle line). When we switch-off current modulation, only a single LS remains in the cavity (blue, top line).

#### D. Multi-Pulse pattern generation

The experiment reported above suggests that a current modulation can be used to obtain a pattern of closely packed localized pulses. This functionality is appealing for many applications like e.g. OCDMA [16] and LIDAR [17], [18], since narrow optical pulses ( $<10$  ps) are typically obtained using conventional PML systems which deliver a periodic train of pulses with no versatility in the pulse arrangement. Pulse patterning can be of course obtained by adding optical gates based on Electro-Optical Modulators, but these solutions are expensive, energetically inefficient, and their implementation requires synchronization between the pulse source and the gating. We implement a pulse pattern generator by driving the system pumping current with a forcing at a period equal to the cavity round-trip and which brings the system into the monostable region where only the periodic pattern of pulses is stable, according to Fig. 2f). The amplitude of the forcing together with the steady value of the bias current, fix the time interval during which the system is driven in this monostable region and, accordingly, this fixes the number of pulses which are excited. For a stable output, the modulation period needs to match closely the cavity round-trip  $\tau$ , which in our case requires a modulation frequency of  $\nu_{mod} = 66.584.030$  Hz. We have verified that a stable output pattern is lost if the frequency mismatch exceeds 10 KHz.

The results obtained are shown in Fig. 6 where we control the number of pulse emitted from one to five by changing

the amplitude of the sinusoidal forcing. The distance between pulses is fixed by the effective temporal extent of the pulses which, as explained above, depends on the carrier recombination time. The close inspection of panel e) and f) reveals that the distance between pulses can change slightly within a pattern. This can be explained by the use of a sinusoidal signal for bringing the system in the monostable region of Fig. 2f), where a periodic pattern of pulses is emitted. In the portion of the sinusoidal signal where this occurs, the current is still increasing, thus leading to an effectively faster carrier recovery rate and therefore to closer pulses. For the same reason, pulse intensities vary slightly inside the pattern. The appearance of an increasing number of pulses for larger amplitudes of the forcing, as well as the inversed phenomenon while decreasing the modulation strength, occurs with an high degree of hysteresis as seen in Fig. 6f), thus revealing multistability between the different situations depicted in Fig. 6a-e)

While Fig. 6 discloses the proof-of-principle of a pulse pattern generator based on localized pulses, more complicated pulse pattern structures can be envisioned using other kind of modulation signals, as square or pulsed current modulation. Even if these modes of operation require to solve the problem of the electrical coupling with the VCSEL, we have tried to use a sinusoidal signal at a period corresponding to  $\tau/2$  for addressing two patterns of pulses within the cavity. The result is shown in Fig. 7, where two localized pulses are separated by half of the round-trip time, in correspondence

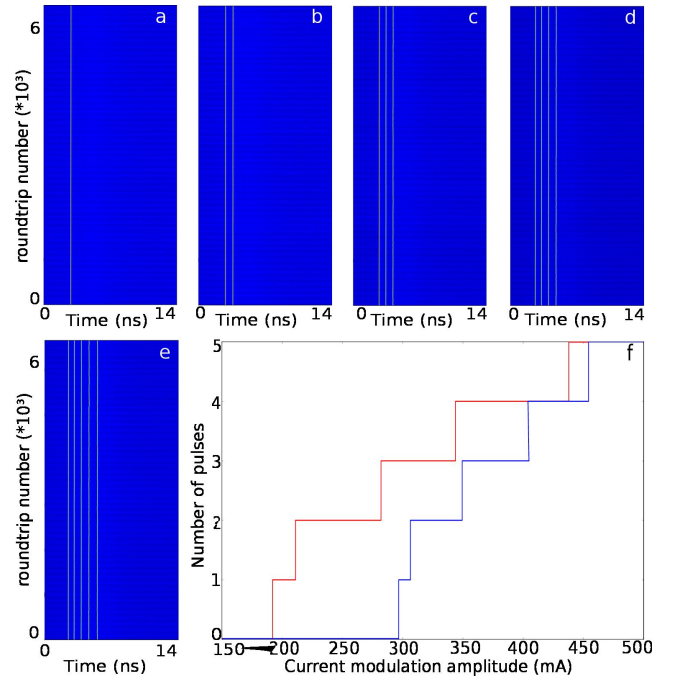


Figure 6. Modulation of the bias current can be used to address temporal LS in the cavity.  $J = 210$  mA,  $\tau = 14.8$  ns,  $\nu_{mod} = 1/\tau$ . As the modulation peak-to-peak amplitude is increased a) 297 mA, b) 306 mA, c) 349 mA, d) 405 mA and e) 454 mA, the number of pulses close to the peak of the modulation is incremented by one. f) The reverse sequence appears when decreasing the modulation amplitude. The modulation value at which transition from  $N - 1$  pulses to  $N$  pulses happens is slightly different with respect the modulation value at which the inverse transition from  $N$  pulses to  $N - 1$  occurs, denoting a strong multistability, .

to the modulation peaks.

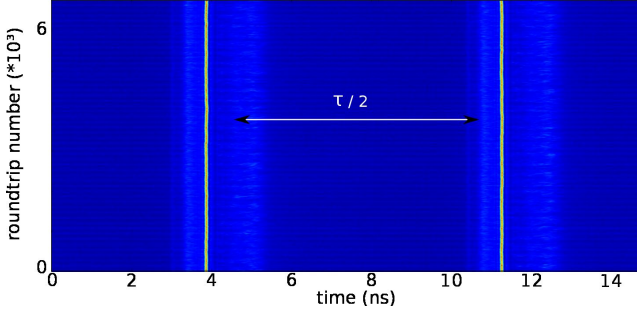


Figure 7. Writing the LS is possible even when the modulation period is set to  $\tau/2$ . The bias is  $J = 210$  mA, and the modulation amplitude 297 mA.

### III. THEORETICAL RESULTS

The proper study and the simulation of PML lasers is a demanding problem from the computational point of view: while pulses may form on a relatively short time scale of a few tens of round-trips, the pulse characteristics only settle on a much longer time scale [29]. If anything, the complex transverse dynamics [20] also present in our case shall slow down the dynamics even further. In particular, we consider here extremely long cavities and therefore very long delays for which with the pulse to round-trip aspect ratio is  $\sim 10^3$ . The necessary presence of noise prevents the use of adaptive step-size algorithms, which would be particularly suitable for such strongly nonlinear problems.

Hence, for the sake of simplicity, we use a purely temporal model as for instance the generic delay differential equation model of [30] which generalizes Haus' model as it encompasses both the pulsating and the steady regimes. While more detailed results could also be obtained with a traveling-Wave approach [31], we found that such a simple model was sufficient to give a good qualitative agreement with the experimental results. Denoting by  $A$  the amplitude of the optical field,  $G$  the gain, and  $Q$  the saturable absorber losses, the model reads

$$\frac{\dot{A}}{\gamma} = \sqrt{\kappa} \exp \left[ \frac{(1 - i\alpha) G_\tau - (1 - i\beta) Q_\tau}{2} \right] A_\tau - A, \quad (1)$$

$$\dot{G} = g_0 + \Delta g \sin \left( \frac{2\pi t}{\tau_m} \right) - \Gamma G - e^{-Q} (e^G - 1) |A|^2, \quad (2)$$

$$\dot{Q} = q_0 - Q - s (1 - e^{-Q}) |A|^2, \quad (3)$$

where time has been normalized to the SA recovery time,  $\alpha$  and  $\beta$  are the linewidth enhancement factors of the gain and absorber sections respectively,  $\kappa$  is the fraction of the power remaining in the cavity after each round-trip,  $g_0$  is the pumping rate,  $\Delta g$  and  $\tau_m$  the amplitude and the period of the modulation of the gain,  $\Gamma$  is the gain recovery rate,  $q_0$  is the value of the unsaturated losses which determines the modulation depth of the SA,  $s$  is the ratio of the saturation energy of the SA and of the gain sections and  $\gamma$  is the bandwidth of the spectral filter. In Eq. 1 the subscript  $\tau$  denotes a delayed value of the variable,  $x_\tau = x(t - \tau)$ . This delay renders the dynamical system infinitely-dimensional and it

describes the spatial boundary conditions of a cavity closing onto itself. As such it governs the fundamental repetition rate of the PML laser. We use standard parameter values that closely represents the experimental situation:  $\kappa = 0.8$ ,  $s = 15$ ,  $q_0 = 0.3$ ,  $\Gamma^{-1} = 66.66$ ,  $\gamma = 3$  and  $\tau = 3000$ . Assuming a SA recovery time of 5 ps, this corresponds to a gain recovery of 333 ps, a bandwidth FWHM of 400 GHz, i.e. 1.3 nm around 980 nm in good agreement with the VCSEL resonance linewidth measurement with a tunable laser and a time delay of 15 ns. Importantly, we stress that the existence of PML regimes below the lasing threshold is mostly independent of the phase-amplitude couplings which explains while in the past we choose  $\alpha = \beta = 0$  for the sake of simplicity. However, we set here the more realistic values of  $\alpha = 1.5$  and  $\beta = 1$ . The lasing threshold is determined by the pump level  $g_0$  for which the off solution  $(A, G, Q) = (0, \Gamma^{-1}g_0, q_0)$  becomes linearly unstable; in our case it is given by  $g_{th} = \Gamma(q_0 - \ln \kappa)$ . Above threshold, the continuous wave (CW) solution bifurcates supercritically from the off state, but PML is found below threshold where the pulsating branches emerge as saddle-node bifurcation of limit cycles, see [14] for more details.

#### A. Multi-pulse pattern

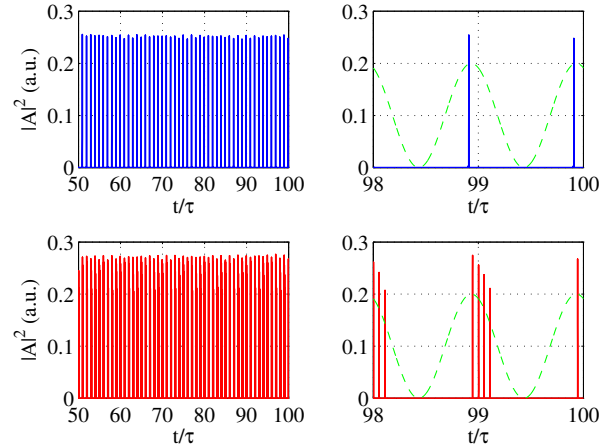


Figure 8. Different co-existing time traces of the temporal intensity over several and two round-trips for  $\Delta g = 0.23$  and  $\tau_m = \tau + 0.2$ . The dashed green lines (not to scale) represent the modulation of the gain.

We set the modulation period very close to the delay value as  $\tau_m = \tau + 0.26$ , the choice of such a precise value will become clear in a moment. The DC bias current is below threshold  $g_0 = 0.8g_{th}$  but also below the minimal current for which LS exists that we denote  $g_{sn} \sim 0.93g_{th}$ . As such, we are in a situation similar to the experiment. We depict our results in Fig. 8 where we evidence the existence of bistability between different temporal patterns composed of either one or three pulses. One clearly see that the pulses organize in the region where the gain is maximal. An inspection of the gain and of the saturable absorption helps to clarify the mechanism of formation of these pulses. During a fraction of the round-trip, the gain is above  $g_{sn}$  while it remains still below  $g_{th}$ . As such one or several pulses can be generated. The pulses do interact

via the gain dynamics which is apparent in the fact that they do not have exactly the same heights. Gain dynamics is known to induce repulsive interaction [27] between pulses. Intuitively, pulses will move toward higher gain, which corresponds to maximizing the distance between them, hence explaining the repulsive nature of the interaction. However, here they cannot move away from each other since the gain varies in time and go below the minimal value at which they can exist. As such, the equilibrium distance between pulses comes for the complex interplay between the repulsive interaction between pulses and the presence of the modulation that acts as an external potential.

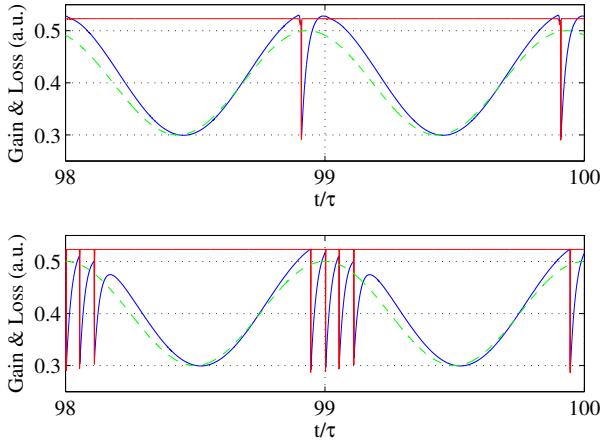


Figure 9. Gain and absorption dynamics for the two co-existing time traces in Fig. 8 over two round-trips with  $\Delta g = 0.23$  and  $\tau_m = \tau + 0.2$ . The dashed green lines (not to scale) represent the modulation of the gain.

A rich multistability diagram for the number of pulse as a function of the gain modulation  $\Delta g$  can be appreciated in Fig. 10, in agreement with experimental results of Fig. 6f). For increasing modulation starting from the off solution, we find in Fig. 10 that small amplitude broad peaks appear for  $\Delta g = 0.2g_{th}$ . This corresponds to the laser reaching exactly threshold at some instant since  $g_0 = 0.8g_{th}$  and such low and broad intensity pulses (not shown) can be interpreted as locally amplified spontaneous emission. The first real LS appears at  $\Delta g = 0.23g_{th}$ . Upon increasing further the modulation amplitude, the pulses energy slowly increases which explains the slope of the plateau (the experiment considering only the pulse number) while the jumps correspond to the apparition of another pulse. Notice in addition that the pulses within a group may have slightly different intensities. Such an information is not apparent in Fig. 10 as we compute the average intensity over a round-trip. Upon decreasing the bias, a strong hysteresis is apparent as in Fig. 6f). Interestingly, one is able to reach much lower values for the modulation amplitude. The value of  $\Delta g = 0.14g_{th}$  corresponds to a maximal gain of  $0.94g_{th}$  which is very close to the value of  $g_{sn}$ , i.e. the minimal value of the current in DC allowing for the existence of a single LS. The diagram in Fig. 10 is normalized in such a way that the integrated intensity of a single pulse at the minimal bias current is unity. We remark that if we have bistability between

1 and 4 pulses, say for instance at  $\Delta g = 0.22g_{th}$ , this certainly implies that we can also have 2 and 3 pulses. As such the diagram of Fig. 10 only gives the extreme envelope of a more complex multi-stable diagram.

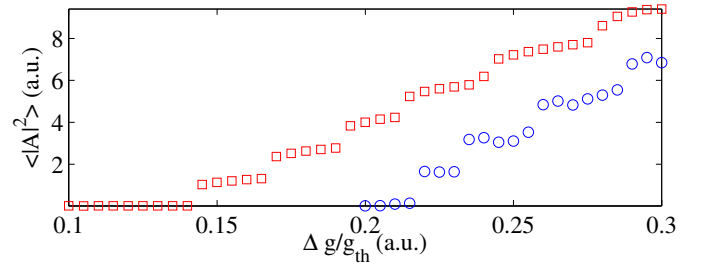


Figure 10. Numerical bifurcation diagram for the pulse number as a function of the modulation of the gain setting  $g_0 = 0.8g_{th}$ . We represent the (normalized) average intensity over a round-trip. The blue circles (resp. red squares) correspond to an upward (resp. downward) scan of the modulation amplitude signaling a strong multi-stability. Each jump corresponds to the appearance of the disappearance of an additional LS.

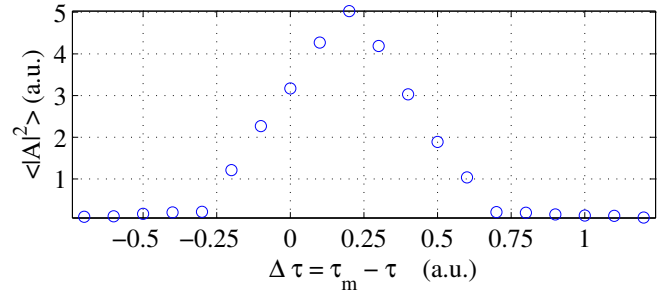


Figure 11. Numerical bifurcation diagram for the pulse number as a function of the detuning of the modulation period as compared to the cavity round-trip. Once notice that a maximal number of pulse is obtained for  $\Delta\tau = 0.23$  which corresponds indeed to the effective round-trip in the cavity dressed by the active medium response time. One notice the sharpness of such a resonance tongue whose width is typically proportional to the pulsewidth.

Experimental results also shown a strong sensitivity of dynamics with respect to the modulation period. We notice that the period of the PML regimes scales as  $T \sim \tau + \gamma^{-1}$ , see [30] for instance. The pulsewidth is proportional to the inverse of the filter bandwidth and there is a deep relation between pulsewidth and deviation of the pulse train period from the value given by the time of flight. One can intuitively consider that  $\gamma$  is the “inertia” of the filter. As such, if a short pulse, say a Dirac delta, is re-injected after a time of flight  $\tau$ , the filter needs a typical time  $\gamma^{-1}$  to filter and re-emit it. In our case, we found that for  $g_0 = 0.8g_{th}$  the fundamental period is  $\tau_m = \tau + 0.26$  which explains why we choose this value in our analysis. We depict in Fig. 11 the sensitivity to the modulation period for a low amplitude modulation of  $\Delta g = 0.23g_{th}$ . One can verify from Fig. 10 that in this case we can have either 1 or 4 pulses. In order to have a simple picture, we start from an initial condition with as many pulses as possible, i.e. the harmonic mode-locking of maximal order found just threshold at  $g_0 = 1.2g_{th}$  in the absence of modulation  $\Delta g = 0$ . Then we suddenly decrease  $g_0$  toward  $g_0 = 0.8g_{th}$  and set the modulation to  $\Delta g = 0.23g_{th}$ . Such a method allows us

to find the maximal number of packed pulse that the system can support as a function of the detuning of the modulation frequency. We see in Fig. 11 that indeed a precise tuning is necessary as the full width of the resonance tongue is 0.5, i.e. of the same order of magnitude than the pulsewidth. Saying that the resonance tongue is of the order of the pulsewidth yields a bandwidth of  $\Delta\nu \sim 10 \text{ ps}/\tau^2 \sim 40 \text{ kHz}$  in good qualitative agreement with the experimental results.

#### IV. CONCLUSIONS

We have shown that electrically biased broad-area VCSELs with optical feedback from a RSAM can be operated in a regime where the passively mode-locked pulses can be addressed and controlled individually when the compound system is operated below threshold. The strong multistability between the off solution and a large variety of pulsating solutions with different number and arrangements of pulses per round-trip, demonstrate that the mode-locked pulses are mutually independent. We show how a modulation of the bias current allows controlling the number of the pulses travelling within the cavity, paving the way an arbitrary pattern generator of picosecond pulses.

#### ACKNOWLEDGMENT

J.J. acknowledges financial support from the Ramon y Cajal fellowship and the CNRS for supporting a visit at the INLN where part of his work was developed as well as useful discussions with H. Wenzel. J.J. and S.B. acknowledge financial support from project RANGER (TEC2012-38864-C03-01) and from the Direcció General de Recerca, Desenvolupament Tecnològic i Innovació de la Conselleria d'Innovació, Interior i Justícia del Govern de les Illes Balears co-funded by the European Union FEDER funds. M.M. and M.G. acknowledge funding of RAGió PACA with the Project Volet GÀrdia 2011 GEDEPULSE and ANR project OPTIROC.

#### REFERENCES

- [1] H. A. Haus, "Mode-locking of lasers," *IEEE J. Selected Topics Quantum Electron.*, vol. 6, pp. 1173–1185, 2000.
- [2] H. A. Haus, "Theory of mode locking with a fast saturable absorber," *Journal of Applied Physics*, vol. 46, pp. 3049–3058, 1975.
- [3] H. A. Haus, "Theory of mode locking with a slow saturable absorber," *Quantum Electronics, IEEE Journal of*, vol. 11, pp. 736–746, 1975.
- [4] R. Fork, C. Shank, R. Yen, and C. Hirlimann, "Femtosecond optical pulses," *Quantum Electronics, IEEE Journal of*, vol. 19, no. 4, pp. 500–506, apr 1983.
- [5] U. Keller, K. J. Weingarten, F. X. Kärtner, D. Kopf, B. Braun, I. D. Jung, R. Fluck, C. Hönninger, N. Matuschek, and J. Aus der Au, "Semiconductor saturable absorber mirrors (SESAM's) for femtosecond to nanosecond pulse generation in solid-state lasers," *Selected Topics in Quantum Electronics, IEEE Journal of*, vol. 2, pp. 435–453, 1996.
- [6] R. Häring, R. Paschotta, A. Aschwanden, E. Gini, F. Morier-Genoud, and U. Keller, "High-power passively mode-locked semiconductor lasers," *Quantum Electronics, IEEE Journal of*, vol. 38, pp. 1268–1275, 2002.
- [7] E. A. Avrutin, J. H. Marsh, and E. L. Portnoi, "Monolithic and multi-GigaHertz mode-locked semiconductor lasers: Constructions, experiments, models and applications," *IEE Proc.-Optoelectron.*, vol. 147, pp. 251–278, 2000.
- [8] P. Stolarz, J. Javaloyes, G. Mezosi, L. Hou, C. Ironside, M. Sorel, A. Bryce, and S. Balle, "Spectral dynamical behavior in passively mode-locked semiconductor lasers (invited)," *Photonics Journal, IEEE*, vol. 3, no. 6, pp. 1067–1082, dec. 2011.
- [9] G. Tandoi, J. Javaloyes, E. Avrutin, C. Ironside, and J. Marsh, "Sub-picosecond colliding pulse mode locking at 126 ghz in monolithic gaas/algaas quantum well lasers: Experiments and theory," *Selected Topics in Quantum Electronics, IEEE Journal of*, vol. 19, no. 4, pp. 1 100 608–1 100 608, 2013.
- [10] J. Javaloyes and S. Balle, "Anticolliding design for monolithic passively mode-locked semiconductor lasers," *Opt. Lett.*, vol. 36, no. 22, pp. 4407–4409, Nov 2011. [Online]. Available:
- [11] M. Xia, M. Thompson, R. Penty, and I. White, "External-cavity mode-locked quantum-dot laser diodes for low repetition rate, sub-picosecond pulse generation," *Selected Topics in Quantum Electronics, IEEE Journal of*, vol. 17, no. 5, pp. 1264–1271, 2011.
- [12] M. Cataluna, Y. Ding, D. Nikitichev, K. Fedorova, and E. Rafailov, "High-power versatile picosecond pulse generation from mode-locked quantum-dot laser diodes," *Selected Topics in Quantum Electronics, IEEE Journal of*, vol. 17, no. 5, pp. 1302–1310, Sept 2011.
- [13] J. Balzer, T. Schlauch, A. Klehr, G. Erbert, G. Trautnknecht, and M. Hofmann, "High peak power pulses from dispersion optimised modelocked semiconductor laser," *Electronics Letters*, vol. 49, no. 13, pp. 838–839, June 2013.
- [14] M. Marconi, J. Javaloyes, S. Balle, and M. Giudici, "How lasing localized structures evolve out of passive mode locking," *Phys. Rev. Lett.*, vol. 112, p. 223901, Jun 2014. [Online]. Available:
- [15] F. Leo, S. Coen, P. Kockaert, S. Gorza, P. Emplit, and M. Haelterman, "Temporal cavity solitons in one-dimensional Kerr media as bits in an all-optical buffer," *Nat Photon*, vol. 4, no. 7, pp. 471–476, Jul 2010. [Online]. Available:
- [16] D. J. R. Hongxi Yin, *Optical Code Division Multiple Access Communication Networks: Theory and Applications*. Springer Science and Business Media, 2009.
- [17] H. B. N. Takeuchi, N. Sugimoto and K. Sakurai, "Random modulation cw lidar."
- [18] K. S. Nobuo Takeuchi, Hiroshi Baba and T. Ueno, "Diode-laser random-modulation cw lidar."
- [19] M. Grabherr, R. Jager, M. Miller, C. Thalmaier, J. Herlein, R. Michalzik, and K. Ebeling, "Bottom-emitting vcsel's for high-cw optical output power," *Photonics Technology Letters, IEEE*, vol. 10, no. 8, pp. 1061–1063, Aug 1998.
- [20] M. Marconi, J. Javaloyes, S. Balle, and M. Giudici, "Passive mode-locking and tilted waves in broad-area vertical cavity surface emitting lasers," *Selected Topics in Quantum Electronics, IEEE Journal of*, vol. PP, no. 99, pp. 1–1, 2014.
- [21] P. Couillet, C. Riera, and C. Tresser, "Stable static localized structures in one dimension," *Phys. Rev. Lett.*, vol. 84, pp. 3069–3072, Apr 2000. [Online]. Available:
- [22] P. Couillet, C. Riera, and C. Tresser, "A new approach to data storage using localized structures," *Chaos*, vol. 14, pp. 193–201, Mar 2004.
- [23] F. T. Arecchi, G. Giacomelli, A. Lapucci, and R. Meucci, "Two-dimensional representation of a delayed dynamical system," *Phys. Rev. A*, vol. 45, pp. R4225–R4228, Apr 1992. [Online]. Available:
- [24] G. Giacomelli and A. Politi, "Relationship between delayed and spatially extended dynamical systems," *Phys. Rev. Lett.*, vol. 76, pp. 2686–2689, Apr 1996. [Online]. Available:
- [25] B. Garbin, J. Javaloyes, G. Tissoni, and S. Barland, "Topological phase bits as reconfigurable memory in a coherently driven laser," *Nature Photonics*, submitted, 2014.
- [26] P. Grelu and N. Akhmediev, "Dissipative solitons for mode-locked lasers," *Nat Photon*, vol. 6, no. 2, pp. 84–92, 2012. [Online]. Available:
- [27] J. Tu and J. Kutz, "Pulse formation, harmonic mode-locking, and stability in actively mode-locked laser cavities," *Quantum Electronics, IEEE Journal of*, vol. 45, no. 3, pp. 282–291, March 2009.
- [28] M. Butkus, E. A. Viktorov, T. Erneux, C. J. Hamilton, G. Maker, G. P. A. Malcolm, and E. U. Rafailov, "85.7 mhz repetition rate mode-locked semiconductor disk laser: fundamental and soliton bound states," *Opt. Express*, vol. 21, no. 21, pp. 25 526–25 531, Oct 2013. [Online]. Available:
- [29] J. Javaloyes and S. Balle, "Mode-locking in semiconductor Fabry-Pérot lasers," *Quantum Electronics, IEEE Journal of*, vol. 46, no. 7, pp. 1023–1030, July 2010.
- [30] A. G. Vladimirov and D. Turaev, "Model for passive mode locking in semiconductor lasers," *Phys. Rev. A*, vol. 72, p. 033808, Sep 2005. [Online]. Available:
- [31] J. Javaloyes and S. Balle, "Freetwm: a simulation tool for multisection semiconductor lasers," <http://onl.uib.es/software>, 2012.





**Mathias Marconi** was born in Nice, France, in 1988. From 2006 to 2011, he was a student at Universitat de Nice Sophia Antipolis (UNS), France. In 2011, he was an exchange student at Strathclyde university, Glasgow, U.K. The same year he obtained the Master degree in optics from UNS. He obtained the Ph.D. degree at the Institut Non-linéaire de Nice, Valbonne, France in 2014. His research interests include semiconductor laser dynamics and pattern formation in out of equilibrium systems. He is a member of the European Physical Society.



**Massimo Giudici** (M'09) received the "Laurea in Fisica" from University of Milan in 1995 and Ph.D from Universitat de Nice Sophia-Antipolis in 1999. He is at present full professor at Universitat de Nice Sophia-Antipolis and deputy director of the laboratory "Institut Non Linéaire de Nice", where he carries out his research activity. Prof. Giudici's research interests revolve around the spatio-temporal dynamics of semiconductor lasers. In particular, he is actively working in the field of dissipative solitons in these lasers. His most important contributions concerned cavity solitons in VCSELs, longitudinal modes dynamics, excitability and stochastic resonances in semiconductor lasers and the analysis of lasers with optical feedback.

concerned cavity solitons in VCSELs, longitudinal modes dynamics, excitability and stochastic resonances in semiconductor lasers and the analysis of lasers with optical feedback.



**Julien Javaloyes** (M'11) was born in Antibes, France in 1977. He obtained his M.Sc. in Physics at the ENS Lyon the PhD in Physics at the Institut Non Linéaire de Nice / Universitat de Nice Sophia-Antipolis working on recoil induced instabilities and self-organization processes in cold atoms. He worked on delay induced dynamics in coupled semiconductor lasers, VCSEL polarization dynamics and monolithic mode-locked semiconductor lasers. He joined in 2010 the Physics Department of the Universitat de les Illes Balears as a Ramon y Cajal fellow. His research interests include laser dynamics and bifurcation analysis.

fellow. His research interests include laser dynamics and bifurcation analysis.



**Patrice Camelin** made a BTS Génie Optique Photonique before continuing his studies at Universitat de Bourgogne (UB) where he obtained his License degree in Physics and His Master degree in Physique Lasers et Matériaux. He is currently a PhD student at the University of Nice Sophia-Antipolis. His research interests include laser dynamics, passive mode-locking and spatially extended systems.



**Daniel Chaparro González** holds the Licenciado degree by the University of Seville. He studied the postgraduate in Germany in the group of Non-linear Photonics of the Institute of Applied Physics of the University of Maastricht, where he worked on laser applications for optical tweezers and manipulation and structuration of fluids. He wrote a thesis entitled "Fabrication of polymer diffraction gratings by means of optically induced dielectrophoresis" with which he obtained the Master of Science degree by the University of Maastricht. Nowadays, he is

a PhD student of the group of Non-linear Waves of the University of the Balearic Islands working in theoretical and experimental aspects of the use of semiconductor lasers to perform remote measurements of distances.



**Salvador Balle** (M'92) was born in Manacor, Mallorca. He graduated in Physics at the Universitat Autònoma de Barcelona, where he obtained a PhD in Physics on the electronic structure of strongly correlated Fermi liquids. After postdoctoral stages in Palma de Mallorca and Philadelphia where he became interested in stochastic processes and Laser dynamics, he joined in 1994 the Physics Department of the Universitat de les Illes Balears, where he is Professor of Optics since 2006. His research interests include laser dynamics, semiconductor optical response modeling, multiple phase fluid dynamics and laser ablation.

response modeling, multiple phase fluid dynamics and laser ablation.